Future Journal of Pharmaceutical Sciences

RESEARCH

Open Access

Enhanced wound healing activity of naturally derived *Lagenaria siceraria* seed oil binary nanoethosomal gel: formulation, characterization, in vitro/in vivo efficiency

Nagham H. Kamal[1], Fatema R. Saber[1*], Abeer Salama[2], Dalia M. N. Abouhussein[3], Soha Ismail[3], Hala M. El-Hefnawy[1] and Meselhy R. Meselhy[1]

Abstract

Background The present study aims to enhance the wound healing potential of the seed oil (SO) of *Lagenaria siceraria* (Egyptian cultivar) via the preparation of SO-loaded binary nanoethosomal (SO-BNE) gels. SO-BNEs were prepared using 2^3 factorial design, characterized for vesicle size, zeta potential, polydispersity index, linoleic and oleic acid EE% for ensuring improved skin permeability. The *L. siceraria* SO, optimized SO-BNE gels (0.5% and 5%) and Mebo® were topically applied in full-thickness wounded rat model twice daily for 10 days.

Results In the SO-BNE gel groups, the normal appearance of the skin architecture and structure of the dermis was revealed. In addition, the levels of NRF2, TGF-β1 and FOXO1, collagen type I, SMA-α and MIP2 were significantly elevated. The wound healing potential of SO-BNE gels was proposed to be via suppression of oxidative stress and stimulation of skin regeneration biomarkers. Furthermore, the SO screening through GC/MS unveiled high percentages of unsaturated fatty acids. SO was also found to be nontoxic to human skin fibroblast cells; enhanced viability and migration rates at concentration of 50 g/mL by 99.76% and 75.9%, respectively.

Conclusion These findings demonstrate that the *Lagenaria siceraria* SO-loaded BNE gels represent a promising delivery for wound healing with enhanced release and bioavailability.

Keywords *Lagenaria siceraria* seed oil, GC–MS, Binary nanoethosomal gel, Wound healing, TGF-β1, Collagen type I

Background

Globally, the management of wounds is extremely challenging and has a significant economic burden on healthcare systems. In 2023, the size of the global market for wound care was estimated at USD 22.25 billion and is expected to grow at a rate of compound yearly growth of 4.17% from 2024 to 2030 [1]. A complicated biological process manages wound healing to restore tissue integrity and function [2]. It involves four overlapping stages: hemostasis, inflammation, proliferation and remodeling. At the early stage of the wound healing process, some cytokines that promote inflammation, including transforming growth factor (TGF) that affects keratinocytes and fibroblasts to stimulate extracellular matrix deposition in the injured area [3] and promote expression of key components such as collagen type I and fibronectin [4].

*Correspondence:
Fatema R. Saber
Fatema.saber@pharma.cu.edu.eg
[1] Department of Pharmacognosy, Faculty of Pharmacy, Cairo University, Cairo 11562, Egypt
[2] Department of Pharmacology, Medical Research and Clinical Studies Institute, National Research Centre, Giza 12622, Egypt
[3] Department of Pharmaceutics, Egyptian Drug Authority (Formerly National Organization for Drug Control and Research), Giza 12553, Egypt

Springer Open

© The Author(s) 2024. **Open Access** This article is licensed under a Creative Commons Attribution 4.0 International License, which permits use, sharing, adaptation, distribution and reproduction in any medium or format, as long as you give appropriate credit to the original author(s) and the source, provide a link to the Creative Commons licence, and indicate if changes were made. The images or other third party material in this article are included in the article's Creative Commons licence, unless indicated otherwise in a credit line to the material. If material is not included in the article's Creative Commons licence and your intended use is not permitted by statutory regulation or exceeds the permitted use, you will need to obtain permission directly from the copyright holder. To view a copy of this licence, visit http://creativecommons.org/licenses/by/4.0/.

However, persistent inflammation is directly related to delayed healing and chronic wounds [5].

The ancient Egyptians had offered approaches for wound healing using natural products [6]. They used honey and grease to reduce inflammation and shield wounds against infection, and lint from vegetable fiber to aid wound drainage.

Throughout history, several wound healing products have been developed, but some are not effective and lead to impaired healing, while many natural products with anti-inflammatory, antimicrobial, antioxidant and collagen-stimulating actions can favor the wound healing processes [7].

Lagenaria siceraria (Mol.) Standley, (known as bottle gourd in English) is an economically important crop belonging to the family Cucurbitaceae. The young and tender fruits of most cucurbits are used as vegetables and demonstrate diverse pharmacological actions [8, 9]. The fruits and seeds of bottle gourd are traditionally used for pain, fever, ulcers, asthma, cough and other bronchial conditions [10]. The seed oil (SO) is known for its high content of unsaturated fatty acids [11], phytosterols [12, 13], polyphenols, vitamins, amino acids and minerals [14]. Most of these constituents are reported to have anti-inflammatory, antimicrobial and antioxidant activities [15–17]. However, their presence in topical preparations is challenging because of their susceptibility to oxidation and water solubility issues.

Several conventional methods for drug delivery are frequently utilized for topical therapies [18], but few of them have few drawbacks like higher dosage required, lower effectiveness and adverse effects [19, 20]. Recently, nano-based transdermal drug delivery systems have been developed to address some of these limitations, enable better bioavailability and patient compliance [21]. Ethosomes are nano-vesicular carriers composed of phospholipid vesicles, water and relatively high amounts of ethanol (a permeation enhancer) to increase the permeation of several lipophilic and hydrophilic drugs [22, 23].

Binary nanoethosome (BNE) is an advanced nano-sized ethosome that contains a binary alcohol phase (ethanol and propylene glycol or isopropanol) to enhance nanoethosome stability. BNE has a deformable spherical structure of lipid bilayer that can permeate deeply into skin layers resulting in enhancement of the transdermal diffusion of the investigated drug through the skin layers [24]. Nano-formulation of seed oil's main advantage is to overcome challenges concerning bioavailability, stability and permeation of the bioactive ingredients [25].

The current study was designed to investigate the wound healing effects of chemically and physically characterized *L. siceraria* SO-loaded BNE gels in rats after detecting the oil's toxicity via an in vitro study. Its effect on the expression of NRF2, TGF-β1 and FOXO1, collagen type I, SMA-α and MIP2 will be investigated. In addition, the metabolic profile of SO will be identified by employing gas chromatography-mass spectrometry (GC–MS).

Materials and methods

Sampling

The SO of *L. siceraria* (Mol.) Standley (Egyptian cultivar) was purchased from Al-Yaqteen private farm, Al-Sharqia, Egypt in July 2022. The SO (100 ml) was prepared from *L. siceraria* seeds (1.0 kg) by cold press method using pressure at 50 °C.

The provisional identification of the plant was performed using Flora & Phytotaxonomic Research Department, Agricultural Museum, Giza, Egypt by Prof. Dr. Abd-Elhalim Abd-Elmogally (Chief Researcher, Flora & Phytotaxonomic Department, Agricultural Museum, Giza, Egypt) with an identification document in Fig. S1A. A voucher specimen (Specimen no. 4.10.2021. II) is preserved at the Pharmacognosy Department Herbarium (Faculty of Pharmacy, Cairo University, Egypt) with a photo of the herbarium shown in Fig. S1B.

Chemicals and reagents

WST-1 reagent (water-soluble tetrazolium salt) and HSF (human skin fibroblasts) were supplied from Nawah scientific research center (El-Mokattam-Egypt). 25% *β*-sitosterol in sesame oil (Mebo® cream), Julphar Gulf Pharmaceutical Industries Manufacture) was purchased from the Egyptian market.

Soybean (90%) was purchased from Thermo Scientific Chemicals (USA). Ethanol 70% was purchased from Fischer Scientific, USA, and propylene glycol (PG) from Sigma-Aldrich, Munich, Germany. Phosphotungstic acid (PTA) and Tween 80 were purchased from Sigma-Aldrich, Munich, Germany. Carbopol 940 from Lubrizol Chemical co, USA, and triethanolamine from Merck, Germany. Ethanolic potassium hydroxide, sodium thiosulfate and phenolphthalein from Merck (Germany).

Methods

Physicochemical characterization of *L. siceraria* SO

Determination of specific gravity

A dry density bottle with a 25 mL volume capacity was precisely weighed before filling with distilled water and then reweighed. Similar to the first, a dried density bottle that had been preweighed was filled with oil and reweighed. The specific gravity was calculated as follows:

Specific gravity = Wb + 0—Wb/Wb + w-Wb where, Wb + 0 is the weight (g) of bottle filled with oil, Wb + w is the weight (g) of bottle filled with water and Wb is the weight (g) of the empty bottle [26].

Determination of refractive index

The refractive index of SO was determined employing an Abbe 60 refractometer [27] at 40 °C [28] using direct reading model (60/95) in which the refractive index is read automatically using the Abbe Utilities software.

Determination of saponification value

SO (Two grams) was placed in a conical flask with ethanolic potassium hydroxide solution (25 mL) and then refluxed for 30 min. Phenolphthalein (2.0 mL) was added after cooling to the saponified mixture followed by titration with 0.5 M HCl [29].

Where N is the molarity of HCl, W is the weight of oil and V1 and V2 are the titer volumes of the blank and sample, respectively, the saponification value is equal to 56. 1 N (V1–V2)/W.

Determination of iodine value

An amount of SO (0.20 g) was dissolved in 10 mL carbon tetrachloride and then 25 mL of Wijs (iodine monochloride) solution was added. The mixture was kept in the dark at 25 ℃ for 30 min. Then, 100 mL of distilled water and 15 mL of potassium iodine solution were added and properly combined. 0.1 M sodium thiosulfate was used to titrate the mixture and 1% starch was used as an indicator [30].

Iodine value = 12.692 (TB–TS) × N/Weight of the oi sample. Where N is the normality of sodium thiosulfate, TB and TS are the titer volumes of the blank and sample, respectively.

Determination of acid value

SO (5 gm) was added to a conical flask containing neutralized boiled alcohol (50 mL). Following this, 5 drops of phenolphthalein were added, using 0.1 M NaOH as a titrant with phenolphthalein as an indicator [30].

Acid value = N × (TB–TS) × M/Weight of the sample oil where, N is the normality of NaOH, M is the molecular weight of NaOH, TB and TS are the titer volumes of the blank and sample, respectively.

Determination of ester value

The formerly calculated saponification value (refluxing the oil with ethanolic potassium hydroxide solution followed by titration with HCL) is used to subtract the oil acid value (titration with 0.1 M NaOH). Then, ester value is calculated as follows:

Ester value = saponification value-acid value.

Chemical analysis by gas chromatography–mass spectrometry (GC–MS) analysis of *L. siceraria* SO

The preparation of fatty acid methyl esters (FAME) and unsaponifiable part were performed according to El-Said & Amer, [31]. GC1310-ISQ mass spectrometer (Thermo Scientific, Austin, TX, USA) with a capillary column HP-5MS (30 m × 0.25 mm × 0.25 µm film thickness) was employed in sample structure investigation using helium as carrier gas at 1 ml/min flow rate. The temperature of the column oven gradually increased from 230 to 290 °C. The temperature of the MS transfer line was held at 250 °C. Meanwhile, the injector temperature was at 260 °C. Autosampler AS1300 coupled with GC in the split mode was used in samples automatic injection (1 µL). EI mass spectra were held at 70 eV ionization voltages in full scan mode holding the ion source at 200 °C. First, peaks were deconvoluted using AMDIS software (www.amdis.net) then identification of the compounds was performed by comparing their retention indices and mass spectra of NIST 11 and WILEY 09 mass spectral databases [32].

In vitro wound healing effect of *L. siceraria* SO

Cell viability

Sharma et al. [33], described WST-1 assay using an Abcam® kit (ab155902 WST-1 Cell Proliferation Reagent) using HSF, cells were kept in DMEM media with the supplement of 100 mg/mL of streptomycin, 100 units/mL of penicillin and 10% of fetal bovine serum (heat-inactivated) in humidified 5% (v/v) CO_2 atmosphere at 37 °C. 50 ml aliquots of cell suspension (3 × 103 cells) were seeded in 96-well plates and incubated for 24 h in complete media. Another aliquot of 50 µl media containing SO at 50 µg/mL and 100 µg/ml was applied to the cells. After 48 h of SO exposure, cells were subjected to 10 µl WST-1 reagent and after 1 h. the absorbance was measured at 450 nm using a BMG LABTECH®- FLUOstar Omega microplate reader (BMG LABTECH, Germany).

Cell migration assay

Main et al. [34] previously described the cell migration assay in which HSF cells were cultured overnight in 5% FBS-DMEM at 37 °C and 5% CO_2. Horizontal scratches were inserted into the confluent monolayer. Fresh medium was added to the control wells while drug wells in concentrations of 50 and 100 µg/mL were treated with fresh media. Monitoring and photographing the wound closures were performed by phase contrast microscopy after 24 and 48 h of incubation. The acquired images are displayed below and were examined by MII Image View software version 3.7. Mebo® cream (Gulphar Gulf company, Egypt) was used as a positive control, while SO and untreated cells served as the negative control.

Formulation of SO nanoethosomes

2^3 Factorial design was constructed to formulate nanoethosomes using Minitab® 20.4. The percentage

of lecithin soybean (X1), percent of ethanol (X2) and percent of propylene glycol (X3) were chosen as the independent variables whereas the selected dependent variables were vesicle size (Y1) and zeta potential (Y2), polydispersity index (Y3), linoleic acid content (Y4) and oleic acid content (Y5).

Firstly, lecithin soybean (X1, 2% and 3%) was primarily dispersed in water forming a colloidal solution by heating at 40 °C. SO was diluted with the ethanolic solution; that is, 1 gm of the SO was diluted with 5% tween 80 in ethanol to 2 mL. In another vessel, take SO alcoholic solution with tween 80 in ethanol and PG (X2, 20, 10% and X3, 0, 10%) and heat at the same temperature. Then, the organic phase was added to the aqueous phase with continuous stirring [35]. Eight nano-formulations were prepared where four formulations of them were BNEs.

Characterization of nanoethosomes

Determination of entrapment efficiency (EE%) (GC/FID assay of FAME in SO nanoethosomes) The analysis of FAME of *L. siceraria* SO (extracted from SO nanoethosomes was processed using gas chromatography coupled with a flame ionization detector (FID), as well as 30 m long, 0.32 mm diameter and 0.25 µm film thickness, cross-linked with 5% phenyl polysiloxane (HP 5-capillary column, Hewlett Packard, Palo Alto, CA, USA) fused-silica column.

Samples preparation

Extraction of *L. siceraria* SO from SO nanoethosomes was processed as follows: 5mL of nanoethosomes were ultracentrifugated for 1 h at 15,000 rpm at 4 °C using cooling centrifuge (Beckman, Fullerton, Canada). The loaded vesicles were successively sonicated with 20 mLs of *n*-hexane (10*10) for 1 min.

Vesicle size (VS)

VS is a crucial parameter for any nano-formulation. Small VS can promote drug permeability and consequently efficiency of the formulation. The measurement of average VS in conjunction with the polydispersity index (PDI) was performed using a Malvern Zeta sizer (Nano ZS90, Malvern Instrument Ltd., UK). Samples were then diluted with distilled water and measured in triplicates [36].

Zeta potential (ZP) and polydispersity index (PDI)

ZP value is an important constraint that indicates the stability of developed nanoethosomes. Together with PDI, they designate the homogeneity of the prepared formulations. Samples were analyzed by the zeta potential analyzer (Nano ZS90, Malvern Instrument Ltd., Worcestershire, UK). Double distilled water was used in the dilution of all formulations and the mean of three measurements ± SD of each formulation was determined [36].

Selection and characterization of the optimized formulation

The optimized formulation was selected using Minitab® 20.4. The optimization constraints are presented in Table 1 and Fig. S5.

Transmission *electron* microscopy (TEM)

The selected formula was envisioned utilizing TEM (JEM-1230, JEOL Ltd., Japan). The sample was dyed with 1% phosphotungstic acid (PTA) and then left to dry on a carbon-coated grid. Afterward, each specimen was visualized under the microscope at 10–100 k-fold amplification at an increasing voltage of 100 kV [37].

Table 1 Independent variables and observed dependent variables of the SO-BNEs (data represented as mean ± SD)

Formulations	Independent variables			Dependent variables				
	Lecithin soybean(X1) %	Ethanol % (X2)	PG* % (X3)	Vesicles Size (Y1) nm	Zeta Potential (Y2) mV	PDI* (Y3)	EE%* (% of total peak area)	
							Linoleic acid (Y4)	Oleic acid (Y5)
F1	3	20	–	188.6 ± 0.53	− 19.3 ± 1.73	0.48 ± 0.04	37.73	7.9
F2	3	20	10	114.8 ± 0.87	− 22.3 ± 0.43	0.47 ± 0.02	52.37	10.91
F3	3	10	–	227.9 ± 0.95	− 18.2 ± 0.8	0.755 ± 0.04	49.22	6.38
F4	3	10	10	150.3 ± 0.26	− 16.2 ± 1.58	0.595 ± 0.03	44.09	7.39
F5	2	20	–	162.1 ± 0.79	− 19.3 ± 1.8	0.48 ± 0.04	49.9	N. D**
F6	2	20	10	154.4 ± 1.73	− 22.2 ± 1.82	0.457 ± 0.02	49.22	7.07
F7	2	10	–	189.1 ± 1.25	− 19.8 ± 2.33	0.541 ± 0.05	49.43	N. D**
F8	2	10	10	151.2 ± 0.91	− 20.3 ± 1.83	0.384 ± 0.02	49.31	N. D**
Optimization constraints				Minimize	Maximize	Minimize	Maximize	Maximize

**PG* propylene glycol, *PDI* polydispersity index and *EE%* entrapment efficiency %

***N.D* non-detected

Preparation of the optimized SO-BNE gel

Direct method was adopted to prepare the BNE gel where 1% Carbopol 940 was dispersed gently into the BNEs alcoholic dispersion with constant stirring using a magnetic stirrer till obtaining homogenous dispersion. Triethanolamine was then dropped to neutralize the developed gel [38].

Characterization of SO-BNE gel

Both the blank gel and SO-BNEs gels were visually tested then a glass plate was used to press 0.5 g of the gel for 5 min to measure the spreadability of the gel where the diameter of the gel after spreading was documented [39].

Chemical characterization of SO-BNE gel

GC/FID assay technique of the FAME part of the extracted SO from BNE gel was performed according to the above-mentioned method. Extraction of *L. siceraria* SO from BNE gel was executed as follows: 1 gm of gel was dispersed in 20 mls of water then was successively sonicated with 20 mls of hexane (10*10) for 1 min each.

Mechanical properties of SO-BNE gel

Both blank and medicated gels were tested mechanically through a TA-XT Plus Texture Analyzer (Stable Micro Systems, UK) which is equipped with a 5 g load cell. The device analytical probe of 10 mm diameter was inserted into each tested gel for a certain depth (15 mm) at a 1 mm/s rate. Both the gel compressibility and strength (hardness) were detected using the subsequent force-distance curve [40, 41]. Tests were performed in triplicates for each gel.

Rheological properties

The rheological characteristics of SO-BNE gel were investigated to identify the gel appropriateness for application using Brookfield DV III Viscometer at 25 °C ± 0.1 °C using spindle 40 within 0.3–5 rpm. The shear rate (γ) and the shear stress (η) were measured and plotted to fit the power law model for equation [42]:

$$\eta = \mathrm{k}\gamma \mathrm{n}^{-1} \quad (1)$$

The consistency index (k) and the flow index (n) of each formula were calculated.

Occlusion factor

The occlusion factor for both blank and SO-BNE gel were revealed. Glass vials were filled with a specified volume of distilled water, weighed then capped with filter paper (cellulose acetate filter, 90 mm, cutoff size 4–7 µm) using adhesive tape as a seal. The tested gel (200 mg) was spread consistently on the filter paper and was kept at 32 °C for 48 h A control vial was used without putting the sampled gel on the filter paper. The vials were reweighed after the specified time to determine evaporated water through the filter. The occlusion factor (F) was calculated as follows [43]:

$$F = (A - B)/A\,X\,100 \quad (2)$$

where A is the water loss without a sample.

B is the water loss with a sample.

In vivo wound healing effects of *L. siceraria* SO and *L. siceraria* SO-BNE gel

Animals

Thirty-two mice of both sex with weights between 25 and 35 g and thirty-six male Sprague Dawley rats of a breeding colony weighing 150–170 g were obtained from the unit of the National Research Centre (NRC), Egypt. The rats were housed at controlled humidity and temperature (45–55% relative humidity/23 ± 2 °C) and exposed alternatively to 12 h. of darkness and light. They were fed with pelleted food and tap water ad libitum and kept in individual clean cages during the experiment period. This study was approved by the Medical Research Ethics Committee, Cairo University, Cairo, Egypt (approval number MP 3256).

Skin irritation study

Thirty-two mice of both sex with weights between 25 and 35 g were used in investigating the irritant effect of *L. siceraria* SO and SO-BNE gel (at concentrations of 5% & 10%) that were applied once. They were divided into 4 groups (eight mice in each and divided equally between males and females). They were caged separately and provided with normal food [44].

Group I: positive control group in which mice weren't given any of the formulation treatments.

Group II Animals were applied by *L. siceraria* SO.

Group III Animals were applied by SO-BNE gel in concentration of 5% of SO.

Group IV Animals were applied by SO-BNE gel in concentration of 10% of SO.

After anesthetizing the mice, hair was removed from its back by depilatories to mark an area of 2 cm^2. Skin reactions and irritations in the form of redness were assessed after 1, 24 and 48 h.

Experimental design of wound

The experiment followed the ARRIVE guidelines and according to the U.K. Animals (Scientific Procedures) Act, 1986 and associated guidelines. Full-thickness wound model in rats was used in the biological evaluation of the topical application of *L. siceraria* SO-BNE gel [45]. Rats were subjected to dorsal skin shaving with an

electric razor under light anesthesia. Afterward, divided into six groups (6 rats each). The normal control group and the remaining five groups were wounded using a sterile biopsy punch needle (No.5, Ribbel International Ltd., India) to create full-thickness skin excision round wounds (5 mm in diameter). One wound was created on both sides of the rats' spinal column by removing a small skin patch to expose the muscular fascia [46].

The wounds were treated after excision, twice daily with reference drug Mebo®, *L. siceraria* SO, *L. siceraria* SO-BNE gel (0.5%) and *L. siceraria* SO-BNE gel (5%). In addition, the untreated group represented a positive control. On the 10-day post-wounding, cervical dislocation was used in rats scarifying after anesthetizing again. After excision of the wounded tissues, they were split up into two parts. Part I was homogenized and the supernatant was used for further biochemical examinations, and part II was used for histopathology.

Morphology of the wound

Wound healing was assessed by measuring the wound area reduction 0, 3, 7 and 10 days after the beginning of the experiment. The relative wound area reduction was calculated using the following equation:

Relative reduction in wound area (%) = (Ao-At) × 100/Ao.

Where Ao and At are the wound area at zero time and time (*t*), respectively. Smart Phone camera Huawei FLA-LX1 (resolution of 8 megapixels) was used in taking photographs of the wound, and then processed on ImageJ (http://rsbweb.nih.gov/ij/download.html) [47].

Evaluation of NRF2, TGF-β1, FOXO1, collagen type I, SMA-α and MIP2

On the 10-day post-wounding, wounded tissues were excised after scarifying the rats. Homogenates of the tissues in 20% (w/v) were prepared in phosphate buffer (pH 7.4) using a homogenizer (Medical instruments, MPW-120, Poland). The homogenates were then centrifuged for 10 min at 4000 rpm and 4 °C using a cooling centrifuge (2 k 15, Sigma, Germany). Supernatants were collected and relevant biochemical markers were evaluated [48].

The levels of NRF2, TGF-β1, collagen type I, SMA-α and MIP2 were determined using enzyme-linked immunosorbent assay (Sunlong Biotech Co., Ltd, China), and FOXO1 was estimated using SunRed Biotech Co., Ltd., China ELISA kit [49].

Histopathological examination by light microscope

10% Formal saline was used in skin samples fixation for at least 24 h and then were preserved in 70% ethanol. Xylene was used in specimens clearing, after that was embedded in paraffin for 24 h in a hot air oven at 56 °C. Beeswax paraffin tissue blocks were sectioned at 4 microns thickness using sledge microtome. These tissue sections were collected on glass slides, deparaffinized and stained by hematoxylin & eosin for routine examination. Images were taken at the pathology laboratory, National Research Centre using an image analysis system with light microscope Olympus CX41 and SC100 video camera attached to a computer system. Photomicrographs were captured at different magnifications and processed using Adobe Photoshop version 8.0.

Statistical analysis

All quantifiable comparisons in our study were performed using one-way analysis of variance (ANOVA) followed by post hoc multiple t-tests for the in vitro assay and Fisher's LSD test using the GraphPad Prism program 8.0, USA, for the in vivo model. Results are presented as mean ± SD of six rats, and the difference was found significant when p value is ≤ 0.05.

Results

Analysis of physicochemical properties

Table S1 summarizes the physicochemical properties of *L. siceraria* SO. The specific gravity of SO was 0.9202. Similar results were previously reported for the SO of *L. siceraria* by Popoola et al. [50], and for pumpkin SO by Amin et al. [51]. The refractive index value of SO is 1.4720. *L. sacraria* SO was found to have high saponification and iodine values of 193.26 and 110.39 (g I_2/100 g oil), respectively. In addition, *L. siceraria* SO was observed to have a low peroxide value of 0.984 meq/kg.

In vitro wound healing effect of *L. siceraria* SO

Effect of L. siceraria SO on cell viability

The effect of *L. siceraria* SO on the viability of HSF was assessed by WST-1 assay (at concentrations of 50 and 100 µg/mL). Generally, SO is regarded to be nontoxic to HSF cells if the cell viability percentage reaches 70% [53]. Both oil concentrations at 50 and 100 µg/mL showed high HSF cell viability percentages: 99.76% and 97.95%, respectively.

Cell migration assay

Cell migration percentages of HSF after treatment with SO for 24 and 48 h are displayed in Fig. S2, while Fig. S3 shows the images of cell migration progression of HSF cells at 50 µg/mL at 0, 24 and 48 h post injury compared to negative and positive controls. There was a mild migration rate percentiles of cells found in negative control with (52.88% ± 4.42), while an enhanced migration of cells was noticed in the positive control (Mebo® cream) group (cell migration rate of 94.96% ± 1.09 after incubation for 48 h). Also, *L.*

siceraria SO showed an enhanced migration rate of 75.9% ± 0.93 after incubation for 48 h. Interestingly, it was observed that the cells migrated better at 50 µg/mL than 100 µg/mL in all samples. It is noteworthy to mention that this is the first time to test the effect of *L. siceraria* SO on HSF cell lines.

GC–MS analysis of L. siceraria SO

GC–MS analysis of the metabolites of *L. siceraria* SO (Fig. S4) led to the annotation of 25 metabolites as compiled in Table S2A and B belonging to fatty acid methyl esters (FAME) and unsaponifiable part (fatty alcohol, fatty aldehydes, aliphatic hydrocarbons and sterols), respectively. 14 FAME were detected that represented 93.23% of the total ionic chromatogram (TIC) area of which 70.17% were calculated as unsaturated fatty acids. They were mostly represented by the omega FAs either monounsaturated such as oleic acid (C18:1) or polyunsaturated such as ϕ-6 linoleic (C18:2) or ϕ-3 linolenic acids (C18:3) representing 12.35, 55.48 and 0.7% area of TIC, respectively. Concerning saturated fatty acids, *L. siceraria* SO was found to be an important source of hexanoic, stearic (C18:0) and palmitic acids (C16:0). In addition, *L. siceraria* SO was found to be a rich source of squalene (representing 5.6% of TIC area). These results are in accordance with that previously reported on *L. siceraria* SO [54].

Formulation of SO nanoethosomes

Table 1 displays the formulation of eight SO nanoethosomes by the 2^3 factorial design where four of them were BNE, the observed dependent variables namely, VS, ZP, PDI and linoleic and oleic acids EE%.

Physicochemical characterization of SO nanoethosomes

Determination of entrapment efficiency (EE%)

After extraction of *L. siceraria* SO from nanoethosomes, GC/FID analysis of the FAME part was employed. The results showed that Lecithin soybean % significantly affected the EE% of oleic acid as presented in Fig. 1. Moreover, F2 exhibited the highest entrapped percentage of both linoleic and oleic acids; 52.37% and 10.91%, respectively, as shown in Table 1.

Measurement of vesicle size (VS)

Table 1 shows the VS of the prepared SO nanoethosomes where VS varied between 114.8 ± 0.87 and 227.9 ± 0.95 nm. It was revealed that using PG in BNEs significantly reduced the vesicle size (Fig. 1).

Zeta potential (ZP) and polydispersity index (PDI)

As presented in Table 1, ZP ranged from −16.2 ± 1.58 to −22.3 ± 0.43 mV. Binary nanoethosomes containing PG showed results above 20 mV indicating the capability of vesicle charges to prevent agglomeration and thus increased stability than other prepared nanoethosomes [55].

All formulations showed PDI less than 1 (as presented in Table 1) where BNE ranged from 0.384 to 0.541, while other nanoethosomes ranged from 0.48 to 0.755. BNEs showed narrower distribution and uniformity of size within formulation than nanoethosomes [56].

Characterization of the selected formulation

F2 was selected as the optimized formulation to continue further studies on it as it has the least VS, PDI, highest linoleic, oleic acid content and ZP as presented in Fig. S5.

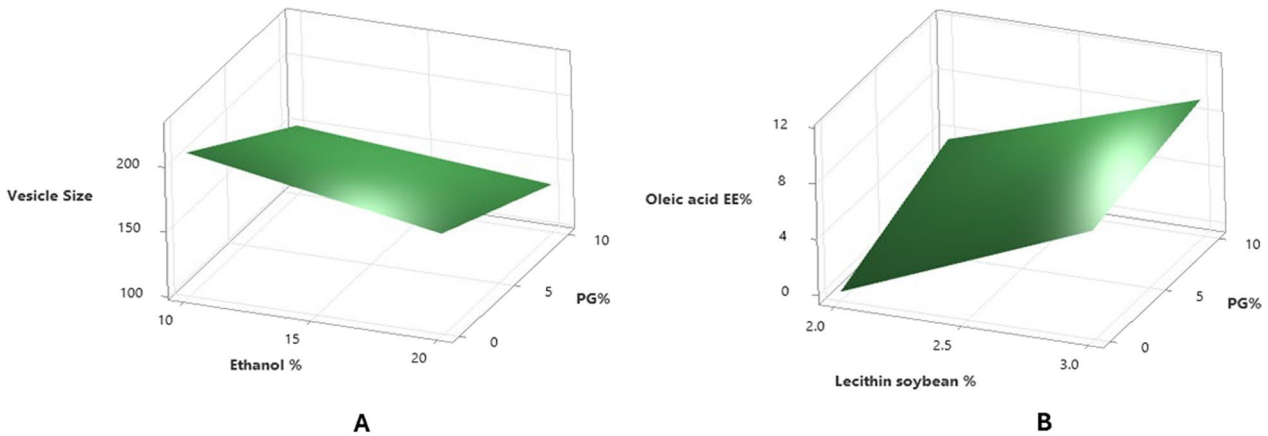


Fig. 1 Surface plot of **A** Vesicle size using different concentrations of ethanol and PG, **B** Oleic acid content using different concentrations of lecithin soybean and PG

Transmission electron microscopy (TEM)

TEM of the selected BNE (F2) is presented in Fig. 2 which shows nanosized non-aggregated vesicles having a bilamellar spherical structure that conforms with the BNE phospholipid vesicular structures.

Preparation of selected SO-BNE gel

1% Carbopol 940 gel was formulated to contain F2 dispersion. The gel formation and cross-linking characteristics of Carbopol 940 make it appropriate for the incorporation of SO-BNE [57].

Characterization of selected SO-BNE gel

The developed SO-BNE gel formulation displayed good homogeneity and consistency. In addition, it showed appropriate spreadability (5.831 ± 0.41 cm), rendering the gel suitable for skin application to guarantee patient compliance.

Chemical characterization of selected SO-BNE gel

The prepared BNE gel of F2 showed appropriate chemical content of extracted SO by 50.4% and 7% of linoleic and oleic acids, respectively.

Mechanical characterization

The inclusion of SO-BNE dispersion into the gel boosted both the gel hardness and compressibility from 9.4 ± 1.3 N to 12.4 ± 1.85 N and from 28.2 N mm to 37.2 N mm, respectively, indicating adequate gel consistency and strength to apply the gel at the site of action without deformation [23].

Occlusion factor

The SO-BNE gel (75.1% ± 1.1%) displayed a significantly higher occlusion factor than the blank gel (59.8% ± 3.4%), indicating good wound healing capability.

Rheological characteristics

Detection of the rheological characteristics of semisolid dosage forms is vital for understanding and controlling how a fluid will perform upon application. It was observed that increasing the shear rate from 3.75 to 37.5 s^{-1} reduced the determined viscosity from 43,077 to 6533 Cps and from 67,231 to 11,760 Cps for SO-BNE gel and blank gel, respectively. Both gels (SO-BNE and blank gels) showed shear thinning properties with a flow index (*n*) value of less than 1. SO-BNE gel displayed non-Newtonian behavior of n value equal to 0.064 and consistency index (*K*) of 3.0736 representing a shear thinning gel of adequate viscosity. On the other side, the blank gel showed a flow index '*n*' of 0.0525 with a consistency index (*k*) of 3.3433 [58].

In vivo wound healing effects of *L. siceraria* SO and *L. siceraria* SO-BNE gel

Skin irritation study

Skin irritation studies of *L. siceraria* SO and SO-BNE gel in a concentration of 5% were found to be compatible with mice skin; there were no signs of erythema or edema formation in rats for a period of 48 h. Meanwhile, SO-BNE gel in concentration of 10% showed slight erythema as shown in Fig. S6 and hence, SO-BNE

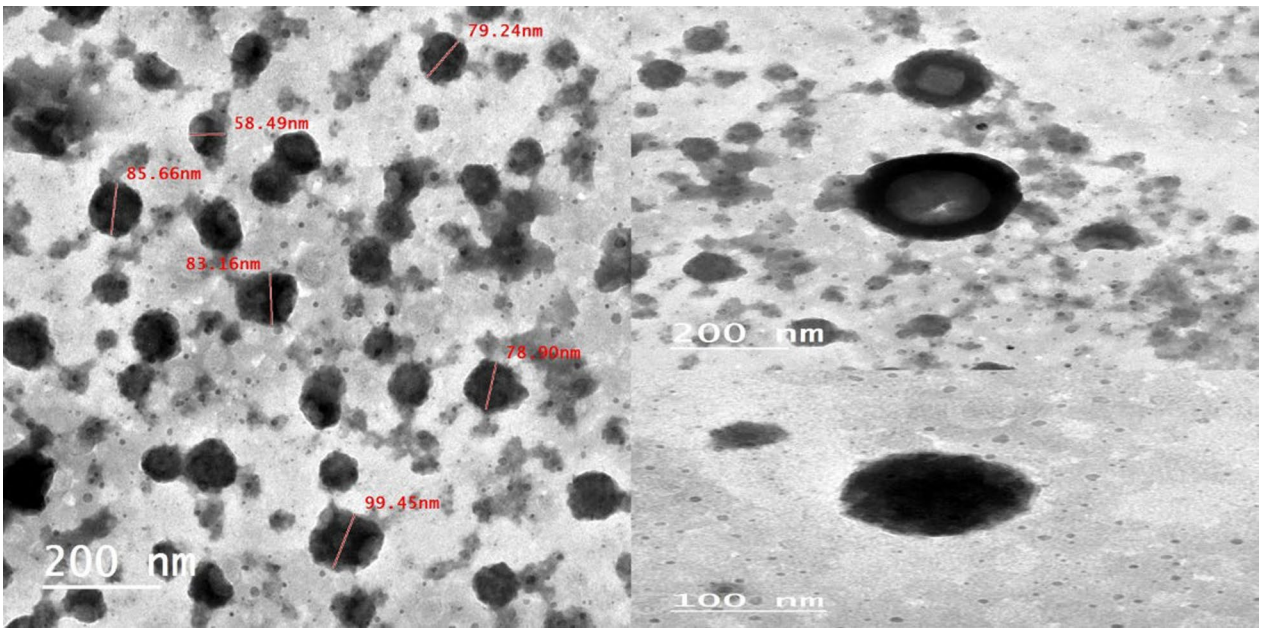


Fig. 2 TEM of the selected SO-BNE (Formula 2)

gel in concentration of 5% and its one-tenth concentration (0.5%) were investigated for their wound healing potentials.

Effect of L. siceraria SO and L. siceraria SO-BNE gel on the wound healing %

An un-healed open contracted wound was observed after 10 days in the positive control group, whereas applying Mebo®, *L. siceraria* SO, *L. siceraria* SO-BNE gel 0.5% and *L. siceraria* SO-BNE gel 5% for 10 days, ameliorated the wound by 75%, 86%, 95% and 99%, respectively, as compared to the positive control group (Fig. 3, Fig. S7).

Effect of L. siceraria SO and L. siceraria SO-BNE gel on the expression of NRF2, FOXO1 and TGF-β in wound healing model

In the current study, levels of NRF2 were decreased significantly in the full-thickness wound rat model by 60% in comparison with the normal control group. Applying Mebo®, *L. siceraria* SO and *L. siceraria* SO-BNE gels in 0.5% and 5% for 10 days increased the levels of NRF2 by 36%, 56%, 105% and 151%, respectively, as compared to the positive control group. In addition, treatment with *L. siceraria* SO-BNE gel (5%) significantly increased the levels of NRF2 by 85%, as compared to Mebo® ($p < 0.05$) suggesting that *L. siceraria* SO-BNE gel (5%) has a major impact on wound healing via activation of the NRF2 pathway (Fig. 4).

FOXO1 induces keratinocyte migration and proliferation and reduces apoptosis of keratinocytes which improves wound healing. In the present study, levels of FOXO1 and TGF-β were significantly decreased in wounded rats by 88% and 79% in comparison with the normal control group. Treatment with Mebo®, *L. siceraria* SO, *L. siceraria* SO-BNE gels in 0.5% and 5% for 10 days increased the levels of FOXO1 by 3-folds, 4-folds, 4-folds and 5-folds, and TGF-β by 1-fold, 2.2-folds, 2.6-folds and 3.8-folds, respectively, as compared to the positive control group. In addition, treatment with *L. siceraria* SO-BNE gel (5%) significantly elevated the levels of FOXO1 by 57% and TGF-β by 1.4 folds, in comparison to Mebo® ($p < 0.05$). These results confirm the cytoprotecting effect of *L. siceraria* SO-BNE gel against oxidative stress induced by wounds (Fig. 4).

Effect of L. siceraria SO and L. siceraria SO-BNE gel on the expression of collagen and alpha-smooth muscle actin (α-SMA) in wound healing model

The wounded rats showed a significant decrease in the levels of collagen and α-SMA by 70%, and 73%, respectively,

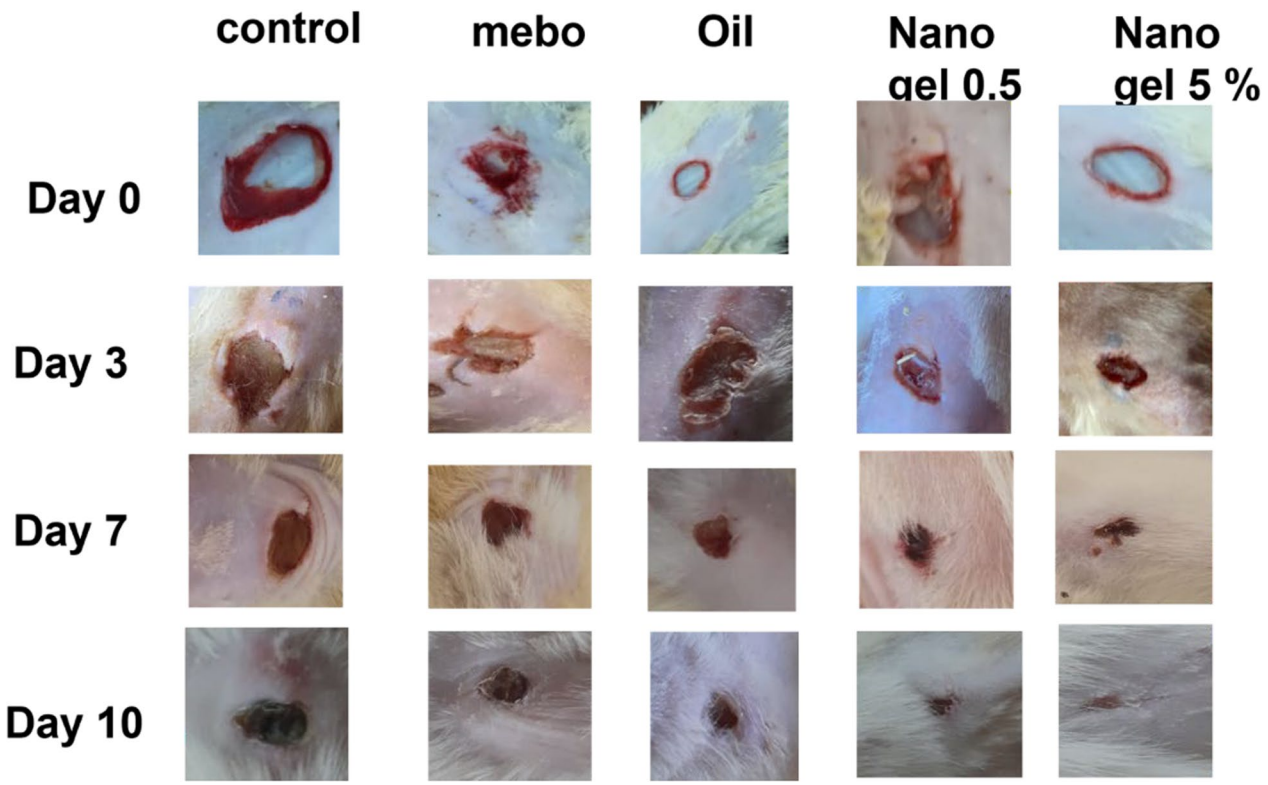


Fig. 3 Effect of *L. siceraria* SO and *L. siceraria* SO-BNE gels and Mebo® on wound morphology in full-thickness wound model

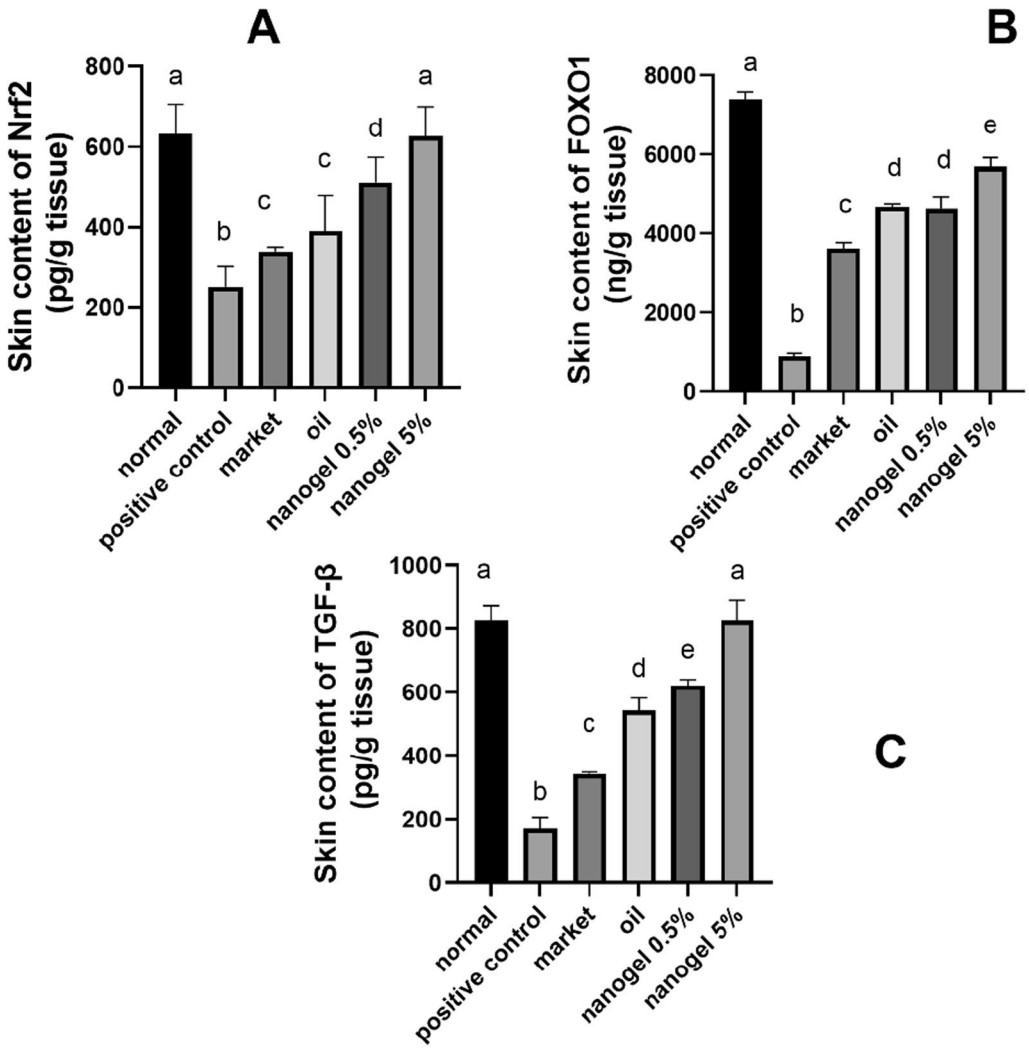


Fig. 4 Effect of *L. siceraria* SO and *L. siceraria* SO-BNE gels and marketed product (Mebo®) on the expression of NRF2 (**A**), FOXO1 (**B**) and TGF-β (**C**) on the 10-day post-wounding. Data are presented as the mean ± SD. of ($n = 6$) for each group. Statistical analysis was carried out by one-way analysis of variance followed by Uncorrected Fisher's LSD test. Same letter means non-significant difference, while different letter means significant difference at $p < 0.05$

in comparison to normal control group. Treatment with Mebo®, *L. siceraria* SO, *L. siceraria* SO-BNE gels in 0.5% and 5% for 10 days could increase the levels of collagen by 34%, 59%, 79% and 104% and α-SMA by 44%, 63%, 212% and 247%, respectively, as compared to the positive control group. Also, treatment with *L. siceraria* SO-BNE gel 5% for 10 days significantly increased the levels of collagen and α-SMA by 1.5 folds and 1.4 folds, respectively, in comparison to Mebo® ($p < 0.05$) (Fig. 5).

Effect of L. siceraria SO and L. siceraria SO-BNE gel on the expression of (Macrophage inflammatory proteins 2) MIP2 in wound healing model

Our results revealed that levels of MIP2 were decreased significantly in rats that were exposed to wound model by 77% in comparison with the normal control group, while treatment with Mebo®, *L. siceraria's* SO and *L. siceraria's* SO-BNE gels 0.5% and 5% for 10 days increased its skin content by 112%, 139%, 162% and 181%, respectively, as compared to the positive control group. In addition, treatment with *L. siceraria* SO-BNE gel 5% significantly increased the levels of MIP2 by 33% as compared to Mebo® ($p < 0.05$) (Fig. S8).

Histopathological results

The histopathological investigation showed that the skin architecture of wounded positive control group was significantly damaged and disrupted (red star) with many inflammatory cells' foci at the wound site with vascular

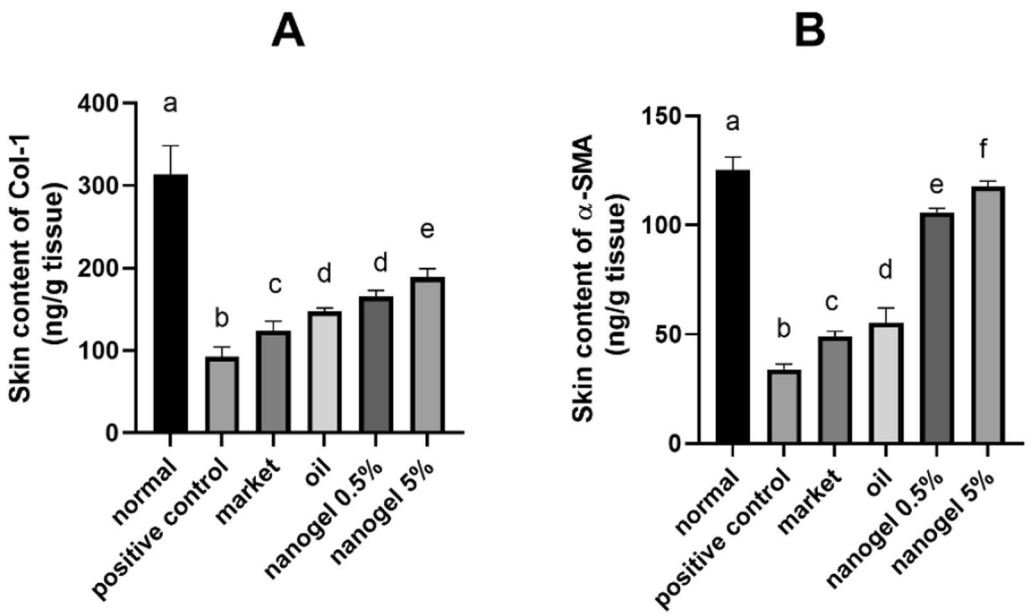


Fig. 5 Effect of *L. siceraria* SO and *L. siceraria* SO-BNE gels and marketed product (Mebo®) on the expression of collagen I (**A**) and alpha-smooth muscle actin (α-SMA) **B** on the 10-day post-wounding. Data are presented as the mean ± SD. of ($n = 6$) for each group. Statistical analysis was carried out by one-way analysis of variance followed by Uncorrected Fisher's LSD test. Same letter means non-significant difference, while different letter means significant difference at $p < 0.05$

changes (red arrows) as shown in Fig. 6B in comparison with normal control group, Fig. 6A. Topical application of *L. siceraria* SO to the positive control group revealed improvement of damaged tissues (black arrows) with normal structure of dermis, well-formed keratinized average thickness of epidermis and remarkable enhancement in average number and thickness of blood vessels, Fig. 6C. Topical application of *L. siceraria* SO-BNE gels (both 0.5 and 5%) when compared to each ingredient alone and to the reference drug could significantly restore the normal skin structure showing normal architecture, well-formed keratinized average thickness of epidermis, normal structure of dermis, average number and thickness of blood vessels and normal appearance of dermal adenexaegular, (yellow arrows) (Fig. 6E, F). These findings indicated that nano-formulation of *L. siceraria* SO had more effective and valuable healing potential for skin wounds than the other treatments.

Discussion

Vegetable oil plays a crucial role in human nutrition and health due to its enrichment in various nutraceuticals. The main obstacles of vegetable oil-based nutraceuticals are concern issues of administration route namely formulation, stability, bioavailability and permeation [25]. Nano-formulation has opened up a new avenue for overcoming these challenges with promising results [59]. Determination of SO proximate parameters is of high priority for assessing its quality in terms of deterioration and oxidation [60]. High saponification and iodine values indicate fatty acids with higher molecular weight and unsaturated fatty acids extent, respectively [61, 62]. Moreover, the SO peroxide value indicates a low degree of oxidation, hence this oil becomes more resistant to oxidation [63]. Chemical profiling of *L. sacraria* SO was performed using GC/MS that resulted in the annotation of 25 metabolites where unsaturated fatty acids constituted the most abundant part, in particular, linoleic acid. The quality of seed oil is correlated with its fatty acid composition, especially the unsaturated fatty acids [64].

Wounds are one of the underreported health issues and a major challenge to healthcare systems being associated with significant costs especially the chronic ones [65]. Chronic wounds which have a duration of 3 weeks or longer are reported to be prevalent globally at 2.5 per 1000 population [66]. The process of wound healing is one that gives rise to tissue repairing in which lost tissue is replaced with a new one [67]. Interestingly, the scope of wound healing by *L. siceraria* is not formerly investigated such that only one study has been reported by Alazzawi [68]. In other studies, *L. siceraria* demonstrated tissue regenerative actions to hepatocytes in addition to antioxidant potentials [69]. Based on in vitro and in vivo studies, *L. siceraria* SO may be regarded as a nontoxic potential wound healer. *L. siceraria* SO in both concentrations of 50 and 100 µg/mL showed no toxicity to HSF

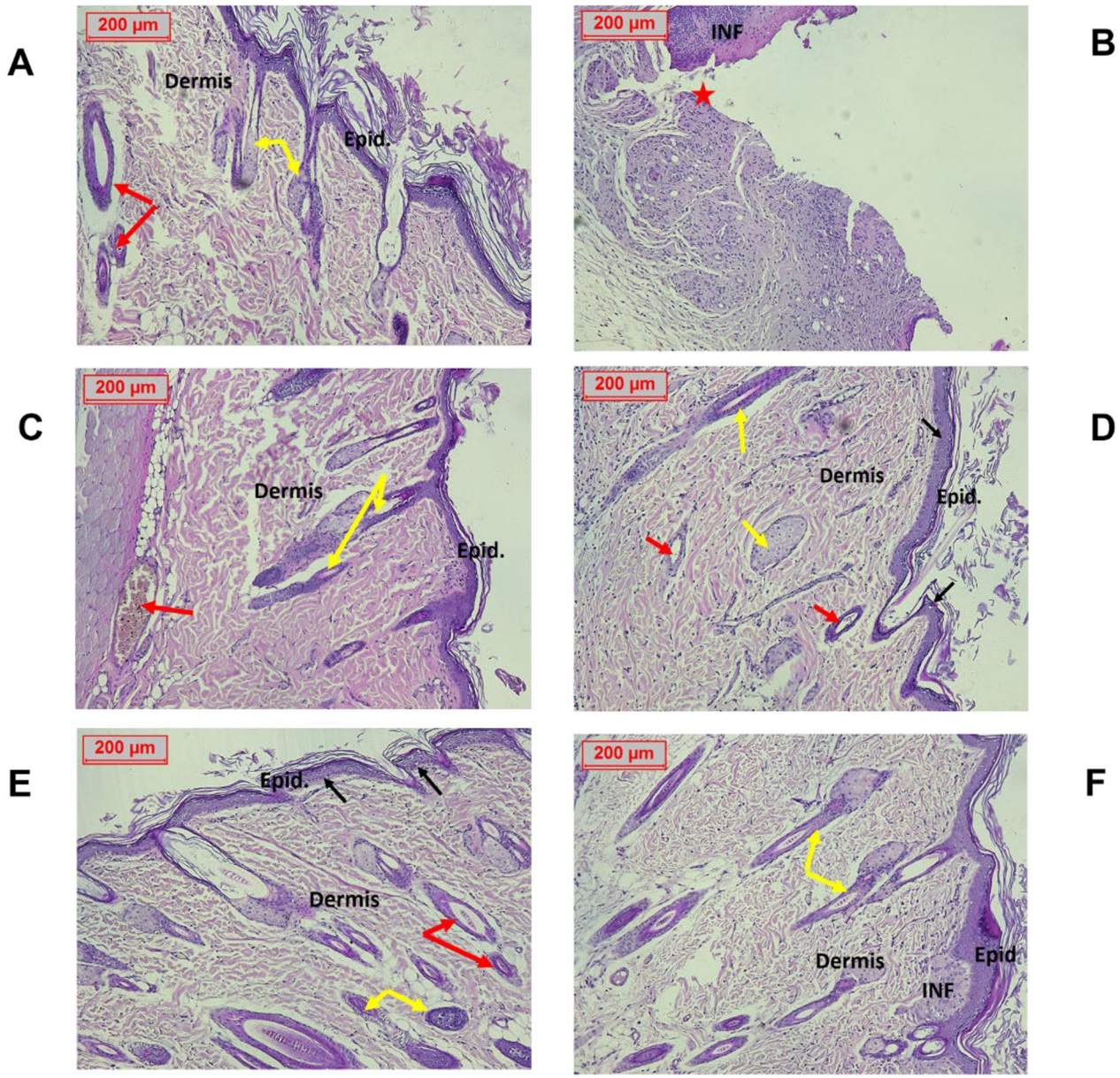


Fig. 6 Histopathological estimation for **A** Normal Group, **B** Positive control wounded group, **C** Oil reference group, **D** Mebo® reference group, **E** *L. siceraria* SO-BNE gel (0.5%), **F** *L. siceraria* SO-BNE gel (5%). H&E 100x. (Epid.): epidermis, (INF.): inflammatory cells red arrows: blood vessels, yellow arrows: dermal adenexa, red star: disrupted architecture of skin, black arrows: cells showing degenerative changes

in terms of high cell viability percentages via WST-1 assay. In vitro cell migration assay was employed to measure the wound closure progression of SO [70] which revealed an enhanced migration rate within 48 h incubation when compared to a reference drug (Mebo® cream).

However, due to water insolubility, SO bioavailability and activity may be limited. Hence, eight SO nanoethosomes were prepared by the 2^3 factorial designs where four formulations were BNEs. Among different formulations, F2 BNE exhibited the highest oil EE% of omega fatty acids, ZP, least VS and PDI. Physically, measured VS, ZP and PDI are important factors that ensure targeting efficiency, stability, and uniformity of vesicles in the prepared BNEs. The use of ethanol in BNEs reduced VS to a suitable range [71] because of phase formation with permeating hydrocarbon as well as reduction of the lipid main transition temperature which leads to fractional fluidization of the formed vesicles. The addition of PG to the ethanolic phase led to a significant reduction in VS which can be attributed to PG fluidizing ability that

facilitates its infiltration into the vesicular fatty bilayer resulting in reduced vesicle size [72]. The morphology of the prepared vesicles in the selected BNE clarifies that no aggregates were detected indicating the homogeneity of the formulation [73]. Therefore, formula 2 was selected to be incorporated into nanoethosomal gel that was formulated using *L. siceraria* SO-loaded BNE for easy skin application and rapid drug penetration through the skin in an attempt to guarantee patient compliance [74]. In our study, further physiochemical characterization of the developed SO-BNE gel formulation was performed to ensure displaying good homogeneity, consistency and spreadability with appropriate chemical content. Chemically, GC/FID analysis resulted in the detection of 50.4% and 7% of linoleic and oleic acids markers, respectively. Physically, mechanical, and rheological characterization in addition to the occlusion factor of the SO-BNE gel were explored. There was a remarkable effect of the inclusion of SO-BNE dispersion into the gel in terms of boosting both the gel hardness and compressibility. Gel hardness is considered the required force to attain gel deformation which can be a good indicator for the ease of gel application at the site of action [42]. Alternatively, compressibility is the work required in compressing the gel through a determined distance. Thus, compressibility expresses how easy to withdraw a gel from its container [41]. Both gel strength (hardness) and compressibility were explored to ensure the appropriateness to use the formulated gel. Skin is a vital parameter to promote the healing of wounds and to enhance the percutaneous penetration of the topically applied formulations. The extent of occlusion employed relies on the nature of the applied dosage form [75]. SO-BNE gel displayed a significantly higher occlusion factor than the blank gel indicating good capability of wound healing. In addition, SO-BNE gel displayed a shear thinning gel of adequate viscosity when compared to blank gel. Therefore, our prepared SO-BNE gel is expected to be suitable for targeting wounded tissues at in vivo conditions.

SO-BNE gels in concentrations of 5% and 0.5% were tested in full-thickness wounded rat model after showing no signs of irritation to mice skin in contrast to 10% that caused slight erythema. Wound healing % was observed in 10 days with a remarkable improvement using SO-BNE gels 5% and 0.5% as compared to the Mebo® and untreated groups. There are several overlapping phases in the wound healing process, beginning with hemostasis and blood clotting. In addition, the production of cytokines and growth factors through migration of some cells into the wound site followed by the neutrophils mediated inflammatory phase as an innate response to the reactive oxygen species (ROS) production. NRF2 has a central role in modulating cytoprotective genes and ROS-detoxifying enzymes [76]. At the same time, FOXO1 inhibits oxidative stress by activating DNA repair enzymes and antioxidant genes. Moreover, FOXO1 stimulates TGF-β activity and upregulates its expression that has a positive effect on wound healing via facilitating keratinocyte migration and downregulates apoptosis [77]. Inflammation has a bad effect on the extracellular matrix (ECM) synthesis as it breaks up its components as collagen and SMA and impairs angiogenesis and re-epithelialization [78]. In the inflammatory phase of wound healing, cytokines have important roles in wound repair, keratinocyte stimulation, fibroblast proliferation and extracellular matrix protein breakdown and synthesis [79]. At the same time, chemokine such as (MIP2) acts as a regulator of leukocyte accumulation at the wound sites and a chemoattractant for monocytes/macrophages during wound healing. In particular, MIP2 participates in neutrophils recruitment to sites of inflammation in many tissues. Its expression can be upregulated by other proinflammatory cytokines, such as IL-1β and TGF-β [80]. Measured NRF2, FOXO1 and TGF-β were remarkably increased in SO-BNE gel by 5% when compared to both Mebo® and untreated positive control groups. In addition, the expression of collagen and α-SMA were significantly upregulated upon applying SO-BNE gel. Histologically, topical application of *L. siceraria* SO-BNE gels (both 0.5 and 5%) when compared to each ingredient alone and to the reference drug could significantly restore the normal skin architecture, the average thickness of the epidermis, the average number and thickness of blood vessels.

This observed promising wound healing potential of *L. siceraria* SO-BNE gel may be attributed to omega fatty acids content in *L. siceraria* SO; linoleic, oleic and α-linolenic acids, in particular. They were proven to mediate antioxidant signaling reactions including nuclear factor erythroid 2-like NRF2 in mouse primary hepatocytes and activate NRF2 signaling that further was found to treat/prevent UVB-induced skin damage, as well [81, 82]. Besides, they elicit opposite effects on inflammation signaling pathways by triggering FOXO1 nuclear localization [83] and inducing the expression levels of some cytokines, e.g., TGF-β1 [84, 85]. In addition, linoleic acid was proven to have a promising effect in the remodeling phase of the healing process through the enhancement of collagen type III conversion to collagen I [86], while oleic acid elevates collagen and MMP-9 expressions [87].

From the aforementioned findings, we can deduce that *L. siceraria* SO wound healing impact can be potentiated through nano-formulation which can be attributed to the small vesicle size and high penetrating effect of the formulated binary ethosomes owing to the high amount of alcoholic content that facilitates the *L. siceraria* SO

to pierce deeply into wound layers that augment the SO potent anti-inflammatory activity [56].

Conclusion

This study presented evidence for the healing potential of *L. siceraria* seed oil on cutaneous wounds that were loaded in a binary ethosomal nano-formulated gel. This is the first unique design of nano-formulation for *L. siceraria* seed oil. An analytical GC/FID approach was employed to chemically characterize the optimized formulation in addition to the other physical characteristics. Based on the GC/MS results, fatty acids/esters represented the most abundant class of detected metabolites in *L. siceraria* seed oil. Much attention has been given to the role of this class in favoring wound healing process especially unsaturated fatty acids like omega-6 linoleic, omega-3 linolenic and oleic acids that have a promising effect in the remodeling phase of the healing process through enhancement of collagen type III conversion to collagen I, in addition to eliciting opposite effects on inflammation signaling pathways and attenuating the expression levels of some inflammatory cytokines.

2^3 factorial design was employed to obtain an optimized BNE. F2 BNE (containing 3% lecithin soybean, 20% ethanol and 10% PG) was selected to be the optimized formulation for having the least VS (114.8 nm), PDI (0.384), highest linoleic acid EE% (52.37%), oleic acid EE% (10.91%) and ZP (-22.3 mV). F2 BNE was incorporated into 1% Carbopol 940 to be appropriate for wound application.

The topical application of *L. siceraria* seed oil BNE gels enhanced the healing process through stimulating NRF2, FOXO1 antioxidant, TGF-β cytokine, ECM components synthesis and suppressing inflammatory process. So, *L. siceraria* seed oil BNE gels, particularly in the concentration of 5% have a positive impact on wound healing in rats. These findings are consistent with our histopathological results. Additionally, the boosted efficacy of formulation containing *L. siceraria* seed oil is attributed to the high penetrating efficacy of the prepared binary nanoethosomal gel that accelerated the anti-inflammatory effect of SO especially fatty acids hence enhancing the release and bioavailability at the site of action. Further clinical studies are needed to clarify the molecular mechanisms for the *L. siceraria* seed oil binary ethosomal nano-formulation.

Abbreviations

AMDIS	Automated mass spectral deconvolution and identification system
ASTM	American Society for Testing and Materials
ARRIVE Guidelines	Animal research: reporting of in vivo experiments
BNE	Binary nanoethosome
DMEM	Dulbecco's modified Eagle medium
ECM	Extracellular matrix
EE%	Entrapment efficiency %
FAME	Fatty acid methyl esters
FBS-DMEM	Fetal bovine serum-DMEM
FOXO1	Forkhead box O
GC–FID	Gas chromatography–flame ionization detector
GC–MS	Gas chromatography–mass spectrometry
HSF	Human skin fibroblasts
IL-1	Interleukin-1
MIP2	Macrophage inflammatory proteins 2
NIST	National Institute of Standards and Technology
NRF2	Nuclear factor erythroid 2
PDI	Polydispersity index
PG	Propylene glycol
PTA	Phosphotungstic acid
α-SMA	Alpha-smooth muscle actin
SO	Seed oil
SO-BNE	Seed oil binary nanoethosome
TEM	Transmission electron microscopy
TGF	Transforming growth factor
TNF	Tumor necrotic factor
USD	United Stated Dollar
VS	Vesicle size
WST-1	Water-soluble tetrazolium salt
ZP	Zeta potential

Supplementary Information

The online version contains supplementary material available at https://doi.org/10.1186/s43094-024-00678-2.

Supplementary Material 1

Acknowledgements

The provisional identification of the plant was performed using the standard flora of Egypt, https://www.semanticscholar.org/paper/Flora-of-Egypt Turril/2f0e4bef5012bf8e3939bc6bdb0a7c187c1eceec, then was kindly identified by Prof. Dr. Abd-Elhalim Abd-Elmogally (Chief Researcher, Flora & Phytotaxonomic Research Department, Agricultural Museum, Giza, Egypt).

Author contributions

Nagham H. kamal contributed to interpreting and writing—original data and design of the study. Fatema R. saber contributed to review—editing and supervision. Abeer Salama contributed to performing animal study and writing—original data. Dalia M N Abou hussein and Soha Ismail contributed to nano-formulation and writing—original data. Hala M. El-Hefnawy and Meselhy R. contributed to review—editing and approval of final version.

Funding

Not applicable.

Availability of data and materials

Data will be made available upon request.

Declarations

Ethics approval and consent to participate

Not applicable.

Competing interests

The author's declared that they have no competing interests.

Received: 7 March 2024 Accepted: 4 August 2024
Published online: 19 August 2024

References

1. https://www.grandviewresearch.com/Industry-Analysis/Wound-Care-Market—Google Search. https://www.google.com/search?q=Https%3A%2F%2FWww.Grandviewresearch.Com%2FIndustry-Analysis%2FWound-Care-Market&sca_esv=9a46615aa720b818&rlz=1C1GGRV_enEG897EG897&ei=ElkvZv21JdqE9u8Pp564uAQ&ved=0ahUKEwj9hpHH_-aFAxVagv0HHScPDkcQ4dUDCBA&uact=5&oq=Https%3A%2F%2FWww.Grandviewresearch.Com%2FIndustry-Analysis%2FWound-Care-Market&gs_lp=Egxnd3Mtd2l6LXNIcnAiRUh0dHBzOi8vV3d3LkdyYW5kdmlld3Jlc2VhcmNoLkNvbS9JbmR1c3RyeS1BbmFseXNpcy9Xb3VuZC1DYXJlL1hcmtldDIQEAAYAxi0AhjqAhiPAdgBATIQEAAYAxi0AhjqAhiPAdgBATIQEAAYAxi0AhjqAhiPAdgBATIQEAAYAxi0AhjqAhiPAdgBATIQEC4YAxi0AhjqAhiPAdgBATIQEC4YAxi0AhjqAhiPAdgBATIQEAAYAxi0AhjqAhiPAdgBATITEC4YAxi0AhjHAxjqAhiPAdgBAUjHHlCeFlieFnACeAGQAQCYAQCgAQCqAQC4AQPIAQD4AQH4AQKYAgKgAmqoAgmYA0q6BgQIARgKkgcBMqAHAA&sclient=gws-wiz-serp. Accessed 29 Apr 2024
2. Saaristo A, Tammela T, Farkkila A et al (2006) Vascular endothelial growth factor-C accelerates diabetic wound healing. Am J Pathol 169:1080–1087. https://doi.org/10.2353/AJPATH.2006.051251
3. Matsuda H, Koyama H, Sato H et al (1998) Role of Nerve Growth Factor in Cutaneous Wound Healing: Accelerating Effects in Normal and Healing-impaired Diabetic Mice. J Exp Med 187:297–306. https://doi.org/10.1084/JEM.187.3.297
4. Miyzono K, Heldin CH (1992) Structure, function and possible clinical application of transforming growth factor-β. Dermatology 19:644–647
5. Dinh T, Tecilazich F, Kafanas A et al (2012) Mechanisms involved in the development and healing of diabetic foot ulceration. Diabetes 61:2937–2947. https://doi.org/10.2337/DB12-0227
6. Shah JB (2011) The history of wound care. J Am Col Certif Wound Spec 3:65–66. https://doi.org/10.1016/J.JCWS.2012.04.002
7. El-Sherbeni SA, Negm WA (2023) The wound healing effect of botanicals and pure natural substances used in in vivo models. Inflammopharmacology 31:755–772. https://doi.org/10.1007/S10787-023-01157-5
8. Ahuja A, Jeong D, Kim MY, Cho JY (2019) *Trichosanthes tricuspidata* Lour. methanol extract exhibits anti-inflammatory activity by targeting Syk, Src, and IRAK1 kinase activity. Evid Based Complement Altern Med. https://doi.org/10.1155/2019/6879346
9. Kwatra D, Dandawate P, Padhye S, Anant S (2016) Bitter melon as a therapy for diabetes, inflammation, and cancer: A panacea? Curr Pharmacol Rep 2:34–44. https://doi.org/10.1007/S40495-016-0045-2/TABLES/1
10. Kumar N, Kale RK, Tiku AB (2013) Chemopreventive effect of *Lagenaria siceraria* in two stages DMBA plus croton oil induced skin papillomagenesis. Nutr Cancer 65:991–1001. https://doi.org/10.1080/01635581.2013.814800
11. Loukou AL, Lognay G, Baudoin JP et al (2013) Effects of fruit maturity on oxidative stability of *Lagenaria siceraria* (molina) standl. Seed oil extracted with hexane. J Food Biochem 37:475–484. https://doi.org/10.1111/j.1745-4514.2012.00657.x
12. Bardaa S, Ben Halima N, Aloui F et al (2016) Oil from pumpkin (*Cucurbita pepo* L.) seeds: evaluation of its functional properties on wound healing in rats. Lipids Health Dis 15:1–12. https://doi.org/10.1186/S12944-016-0237-0/FIGURES/3
13. Thakur M, Vasudeva N, Sharma S, Datusalia AK (2022) Plants and their bioactive compounds as a possible treatment for traumatic brain injury-induced multi-organ dysfunction syndrome. CNS Neurol Disord Drug Targets 22:1313–1334. https://doi.org/10.2174/1871527321666220830164432
14. Essien E, Antia BS, Essien EE et al (2015) *Lagenaria siceraria* (molina) standley. Total polyphenols and antioxidant activity of seed oils of bottle gourd cultivars. World J Pharm Res 4:274–285
15. Reyes-Becerril M, Angulo C, Cosío-Aviles L et al (2022) Cylindropuntia cholla aqueous root rich in phytosterols enhanced immune response and antimicrobial activity in tilapia *Oreochromis niloticus* leukocytes. Fish Shellfish Immunol 131:408–418. https://doi.org/10.1016/J.FSI.2022.10.028
16. Hsu CC, Kuo HC, Huang KE (2017) The effects of phytosterols extracted from diascorea alata on the antioxidant activity, plasma lipids, and hematological profiles in taiwanese menopausal women. Nutrients 9:1320. https://doi.org/10.3390/NU9121320
17. Othman L, Sleiman A, Abdel-Massih RM (2019) Antimicrobial activity of polyphenols and alkaloids in middle eastern plants. Front Microbiol 10:911. https://doi.org/10.3389/FMICB.2019.00911/BIBTEX
18. Carneiro G, Aguiar MG, Fernandes AP, Ferreira LAM (2012) Drug delivery systems for the topical treatment of cutaneous leishmaniasis. Expert Opin Drug Deliv 9:1083–1097. https://doi.org/10.1517/17425247.2012.701204
19. Harris VR, Cooper AJ (2017) Atopic dermatitis: the new frontier. Med J Aust 207:351–356. https://doi.org/10.5694/mja17.00463
20. Patnaik S, Purohit D, Biswasroy P et al (2022) Recent advances for commedonal acne treatment by employing lipid nanocarriers topically. Int J Health Sci (Qassim) 6:180–205. https://doi.org/10.53730/ijhs.v6ns8.9671
21. Tran TNT (2013) Cutaneous drug delivery: an update. J Investig Dermatology Symp Proc 16:S67–S69. https://doi.org/10.1038/JIDSYMP.2013.28
22. Nainwal N, Jawla S, Singh R, Saharan VA (2019) Transdermal applications of ethosomes—a detailed review. J Liposome Res 29:103–113. https://doi.org/10.1080/08982104.2018.1517160
23. Abouhussein DM (2021) Enhanced transdermal permeation of BCS class IV aprepitant using binary ethosome: optimization, characterization and ex vivo permeation. J Drug Deliv Sci Technol 61:102185
24. Zhou Y, Wei Y, Liu H et al (2010) Preparation and in vitro evaluation of ethosomal total alkaloids of *Sophora alopecuroides* loaded by a transmembrane pH-gradient method. AAPS PharmSciTech 11:1350–1358. https://doi.org/10.1208/S12249-010-9509-6/METRICS
25. Yuvashree M, Gokulakannan R, Ganesh RN, Viswanathan P (2019) Enhanced therapeutic potency of nanoemulsified garlic oil blend towards renal abnormalities in pre-diabetic rats. Appl Biochem Biotechnol 188:338–356
26. Kukeera T, Banadda N, Tumutegyereize P et al (2015) Extraction, quantification and characterization of oil from pumpkin seeds. Int J Agric Biol Eng 8:98–102. https://doi.org/10.3965/J.IJABE.20150801.013
27. Horwitz W, Latimer G (2000) Official methods of analysis, 17th edn. The Association of Official Analytical Chemists, Gaithersburg
28. Tsaknis J, Lalas S, Lazos ES (1997) Characterization of crude and purified pumpkin seed oil. Grasas Aceites 48:267–272
29. Ogungbenle HN, Afolayan MF (2015) Physical and chemical characterization of roasted cashew nut (*Anacardium occidentale*) flour and oil. Int J Food Sci Nutr Eng 5:1–7
30. Ogungbenle HN, Omodara OP (2014) Physico chemical and fatty acid composition of nicker bean (*Entada gigas*) seed oil. Adv Anal Chem 4:35–39
31. El-Said ME, Amer MM (1965) Oils, fats, waxes and surfactants. Anglo Egyptian Book Shop, Cairo
32. Taha Mohamed N, Abdelsalam DH, Salem El-Ebiarie A, Elaasser M (2021) Seperation of bioactive compounds from Haemolymph of scarab beetle *Scarabaeus sacer* (Coleoptera: Scarabaeidae) by GC–MS and determination of its antimicrobial activity. Int J Appl Biol 5:98–116. https://doi.org/10.20956/ijab.v5i2.18539
33. Sharma A, Marceau C, Hamaguchi R et al (2014) Human induced pluripotent stem cell-derived cardiomyocytes as an in vitro model for coxsackievirus B3-induced myocarditis and antiviral drug screening platform. Circ Res 115:556–566. https://doi.org/10.1161/CIRCRESAHA.115.303810
34. Main KA, Mikelis CM, Doçi CL (2020) In vitro wound healing assays to investigate epidermal migration. Methods Mol Biol 2109:147–154. https://doi.org/10.1007/7651_2019_235
35. Shetty S, Jose J, Kumar L, Charyulu RN (2019) Novel ethosomal gel of clove oil for the treatment of cutaneous candidiasis. J Cosmet Dermatol 18:862–869. https://doi.org/10.1111/JOCD.12765
36. Abouhussein DMN, El Din B, Mahmoud D, Mohammad FE (2019) Design of a liquid nano-sized drug delivery system with enhanced solubility of rivaroxaban for venous thromboembolism management in paediatric patients and emergency cases. J Liposome Res 29:399–412. https://doi.org/10.1080/08982104.2019.1576732
37. Abdel-All SR, Shakour ZTA, Abouhussein DMN et al (2021) Phytochemical and biological evaluation of a newly designed nutraceutical self-nanoemulsifying self-nanosuspension for protection and treatment of cisplatin induced testicular toxicity in male rats. Molecules 26:408. https://doi.org/10.3390/MOLECULES26020408
38. Garhy DMA, Ismail S, Ibrahim HK, Ghorab MM (2018) Buccoadhesive gel of carvedilol nanoparticles for enhanced dissolution and bioavailability. J Drug Deliv Sci Technol 47:151–158. https://doi.org/10.1016/J.JDDST.2018.07.009
39. Dantas MGB, Reis SAGB, Damasceno CMD et al (2016) Development and evaluation of stability of a gel formulation containing the monoterpene borneol. Sci World J. https://doi.org/10.1155/2016/7394685

40. Gandra SCR, Nguyen S, Nazzal S et al (2015) Thermoresponsive fluconazole gels for topical delivery: rheological and mechanical properties, in vitro drug release and anti-fungal efficacy. Pharm Dev Technol 20:41–49. https://doi.org/10.3109/10837450.2013.846376
41. Jones DS, Woolfson AD, Brown AF (1997) Textural, viscoelastic and mucoadhesive properties of pharmaceutical gels composed of cellulose polymers. Int J Pharm 151:223–233. https://doi.org/10.1016/S0378-5173(97)04904-1
42. Abouhussein DMN, Khattab A, Bayoumi NA et al (2018) Brain targeted rivastigmine mucoadhesive thermosensitive in situ gel: optimization, in vitro evaluation, radiolabeling, in vivo pharmacokinetics and biodistribution. J Drug Deliv Sci Technol 43:129–140. https://doi.org/10.1016/J.JDDST.2017.09.021
43. Montenegro L, Parenti C, Turnaturi R, Pasquinucci L (2017) Resveratrol-loaded lipid nanocarriers: correlation between in vitro occlusion factor and in vivo skin hydrating effect. Pharmaceutics 9:58. https://doi.org/10.3390/PHARMACEUTICS9040058
44. Upadhyay NK, Kumar R, Mandotra SK et al (2009) Safety and healing efficacy of Sea buckthorn (*Hippophae rhamnoides* L.) seed oil on burn wounds in rats. Food Chem Toxicol 47:1146–1153. https://doi.org/10.1016/j.fct.2009.02.002
45. Movaffagh J, Khatib M, Fazly Bazzaz BS et al (2022) Evaluation of wound-healing efficiency of a functional Chitosan/Aloe vera hydrogel on the improvement of re-epithelialization in full thickness wound model of rat. J Tissue Viability 31:649–656. https://doi.org/10.1016/J.JTV.2022.07.009
46. Hussein RA, Salama AAA, El Naggar ME, Ali GH (2019) Medicinal impact of microalgae collected from high rate algal ponds; phytochemical and pharmacological studies of microalgae and its application in medicated bandages. Biocatal Agric Biotechnol 20:101237. https://doi.org/10.1016/J.BCAB.2019.101237
47. Asfour MH, Elmotasem H, Mostafa DM, Salama AAA (2017) Chitosan based pickering emulsion as a promising approach for topical application of rutin in a solubilized form intended for wound healing: in vitro and in vivo study. Int J Pharm 534:325–338. https://doi.org/10.1016/J.IJPHARM.2017.10.044
48. Salama A, Elgohary R (2021) L-carnitine and Co Q10 ameliorate potassium dichromate -induced acute brain injury in rats targeting AMPK/AKT/NF-κβ. Int Immunopharmacol 101:107867. https://doi.org/10.1016/J.INTIMP.2021.107867
49. Salama A, Elgohary R, Amin MM, Elwahab SA (2022) Immunomodulatory effect of protocatechuic acid on cyclophosphamide induced brain injury in rat: modulation of inflammosomes NLRP3 and SIRT1. Eur J Pharmacol 932:175217. https://doi.org/10.1016/J.EJPHAR.2022.175217
50. Popoola YY, Akinoso R, Raji AO (2016) Optimization of oil extraction from giant bushel gourd seeds using response surface methodology. Food Sci Nutr 4:759–765. https://doi.org/10.1002/FSN3.341
51. Amin MZ, Islam T, Mostofa F et al (2019) Comparative assessment of the physicochemical and biochemical properties of native and hybrid varieties of pumpkin seed and seed oil (*Cucurbita maxima* Linn.). Heliyon 5:e02994. https://doi.org/10.1016/j.heliyon.2019.e02994
52. Horwitz W (2000) official methods of analysis, 17th edn. Association of Official Analytical Chemists, Rockville
53. Figueiró LR, Comerlato LC, Da Silva MV et al (2016) Toxicity of *Glandularia selloi* (Spreng.) Tronc. leave extract by MTT and neutral red assays: influence of the test medium procedure. Interdiscip Toxicol 9:25. https://doi.org/10.1515/INTOX-2016-0004
54. Essien E, Udo I, Umoh S (2013) Fatty acids composition and seed oils quality of *Lagenaria siceraria* cultivars grown in Northern Nigeria. Int J Nat Prod Sci 3:1–8
55. Habib BA, Sayed S, Elsayed GM (2018) Enhanced transdermal delivery of ondansetron using nanovesicular systems: fabrication, characterization, optimization and ex-vivo permeation study-Box-Cox transformation practical example. Eur J Pharm Sci 115:352–361. https://doi.org/10.1016/J.EJPS.2018.01.044
56. Zhang JP, Wei YH, Zhou Y et al (2012) Ethosomes, binary ethosomes and transfersomes of terbinafine hydrochloride: a comparative study. Arch Pharm Res 35:109–117. https://doi.org/10.1007/S12272-012-0112-0/METRICS
57. Hajare A, Dol H, Patil K (2021) Design and development of terbinafine hydrochloride ethosomal gel for enhancement of transdermal delivery: in vitro, in vivo, molecular docking, and stability study. J Drug Deliv Sci Technol 61:102280. https://doi.org/10.1016/J.JDDST.2020.102280
58. Chang JY, Oh YK, Choi HG et al (2002) Rheological evaluation of thermosensitive and mucoadhesive vaginal gels in physiological conditions. Int J Pharm 241:155–163. https://doi.org/10.1016/S0378-5173(02)00232-6
59. Zaki NM (2014) Progress and problems in nutraceuticals delivery. J Bioequiv Availab 6:75
60. Oderinde RA, Ajayi IA, Adewuyi A (2009) Characterization of seed and seed oil of *Hura crepitans* and the kinetics of degradation of the oil during heating. Electron J Environ Agric Food Chem 8:201–208
61. Esan YO, Fasasi OS (2013) Amino acid composition and antioxidant properties of African yam bean (*Spenostylis stenocarpa*) protein hydrolysates. Afr J Food Sci Technol 4:100–105
62. Adu OB, Ogundeko TO, Ogunrinola OO et al (2015) The effect of thermal processing on protein quality and free amino acid profile of *Terminalia catappa* (Indian almond) seed. J Food Sci Technol 52:4637–4641. https://doi.org/10.1007/S13197-014-1490-8
63. Haile M, Duguma HT, Chameno G, Kuyu CG (2019) Effects of location and extraction solvent on physico chemical properties of *Moringa stenopetala* seed oil. Heliyon. https://doi.org/10.1016/J.HELIYON.2019.E02781
64. Fayek NM, Farag MA, Saber FR (2021) Metabolome classification via GC/MS and UHPLC/MS of olive fruit varieties grown in Egypt reveal pickling process impact on their composition. Food Chem 339:127861. https://doi.org/10.1016/j.foodchem.2020.127861
65. Frykberg RG, Banks J (2015) Challenges in the treatment of chronic wounds. Adv Wound Care 4(9):560–582
66. Martinengo L, Olsson M, Bajpai R et al (2019) Prevalence of chronic wounds in the general population: systematic review and meta-analysis of observational studies. Ann Epidemiol 29:8–15
67. Melguizo-rodríguez L, de Luna-Bertos E, Ramos-torrecillas J et al (2021) Potential effects of phenolic compounds that can be found in olive oil on wound healing. Foods 10:1642. https://doi.org/10.3390/foods10071642
68. Alazzawi A (2022) Wound healing properties of *Lagenaria siceraria* L. extract and its nanoformulation (Doctoral dissertation, University of Petra (Jordan))
69. Saha P, Mazumder UK, Haldar PK et al (2011) Antioxidant and hepatoprotective activity of *Lagenaria siceraria* aerial parts. Pharmacogn J 3:67–74
70. Liang CC, Park AY, Guan JL (2007) In vitro scratch assay: a convenient and inexpensive method for analysis of cell migration in vitro. Nat Protoc 22(2):329–333. https://doi.org/10.1038/nprot.2007.30
71. López-Pinto JM, González-Rodríguez ML, Rabasco AM (2005) Effect of cholesterol and ethanol on dermal delivery from DPPC liposomes. Int J Pharm 298:1–12. https://doi.org/10.1016/J.IJPHARM.2005.02.021
72. Moolakkadath T, Aqil M, Ahad A et al (2019) Fisetin loaded binary ethosomes for management of skin cancer by dermal application on UV exposed mice. Int J Pharm 560:78–91. https://doi.org/10.1016/J.IJPHARM.2019.01.067
73. Aljohani AA, Alanazi MA, Munahhi LA et al (2023) Binary ethosomes for the enhanced topical delivery and antifungal efficacy of ketoconazole. OpenNano 11:100145. https://doi.org/10.1016/J.ONANO.2023.100145
74. El Maghraby GMM, Campbell M, Finnin BC (2005) Mechanisms of action of novel skin penetration enhancers: phospholipid versus skin lipid liposomes. Int J Pharm 305:90–104
75. Berardesca E, Vignoli GP, Fideli D, Maibach H (1992) Effect of occlusive dressings on the stratum corneum water holding capacity. Am J Med Sci 304:25–28. https://doi.org/10.1097/00000441-199207000-00007
76. Hiebert P, Werner S (2019) Regulation of wound healing by the NRF2 transcription factor—more than cytoprotection. Int J Mol Sci 20:3856. https://doi.org/10.3390/IJMS20163856
77. Hameedaldeen A, Liu J, Batres A et al (2014) FOXO1, TGF-β regulation and wound healing. Int J Mol Sci 15:16257–16269. https://doi.org/10.3390/IJMS150916257
78. Kamel R, Elmotasem H, Abdelsalam E, Salama A (2021) Lepidium sativum seed oil 3D nano-oleogel for the management of diabetic wounds: GC/MS analysis, in-vitro and in-vivo studies. J Drug Deliv Sci Technol 63:102504. https://doi.org/10.1016/J.JDDST.2021.102504
79. Abd El-Alim SH, Salama A, Darwish AB (2020) Provesicular elastic carriers of Simvastatin for enhanced wound healing activity: an in-vitro/in-vivo

study. Int J Pharm 585:119470. https://doi.org/10.1016/J.IJPHARM.2020.119470
80. Badr G, Badr BM, Mahmoud MH et al (2012) Treatment of diabetic mice with undenatured whey protein accelerates the wound healing process by enhancing the expression of MIP-1α, MIP-2, KC, CX3CL1 and TGF-β in wounded tissue. BMC Immunol 13:1–9. https://doi.org/10.1186/1471-2172-13-32/FIGURES/3
81. Cui Y, Wang Q, Yi X, Zhang X (2016) Effects of fatty acids on CYP2A5 and Nrf2 expression in mouse primary hepatocytes. Biochem Genet 54:29–40. https://doi.org/10.1007/S10528-015-9697-6/FIGURES/4
82. Wang SH, Chen YS, Lai KH et al (2022) Prinsepiae Nux extract activates NRF2 activity and protects UVB-induced damage in keratinocyte. Antioxidants 11:1755. https://doi.org/10.3390/ANTIOX11091755/S1
83. Kwon SY, Massey K, Watson MA et al (2020) Oxidised metabolites of the omega-6 fatty acid linoleic acid activate dFOXO. Life Sci Alliance. https://doi.org/10.26508/LSA.201900356
84. Donato-Trancoso A, Monte-Alto-Costa A, Romana-Souza B (2016) Olive oil-induced reduction of oxidative damage and inflammation promotes wound healing of pressure ulcers in mice. J Dermatol Sci 83:60–69. https://doi.org/10.1016/J.JDERMSCI.2016.03.012
85. Yang S, Wang C, Huang X et al (2023) Linoleic acid stimulation results in TGF-β1 production and inhibition of PEDV infection in vitro. Virology 581:89–96. https://doi.org/10.1016/J.VIROL.2023.03.004
86. Silva JR, Burger B, Kühl CMC et al (2018) Wound healing and omega-6 fatty acids: from inflammation to repair. Mediat Inflamm. https://doi.org/10.1155/2018/2503950
87. Cardoso CR, Favoreto S, Oliveira LL et al (2011) Oleic acid modulation of the immune response in wound healing: a new approach for skin repair. Immunobiology 216:409–415. https://doi.org/10.1016/J.IMBIO.2010.06.007

Publisher's Note

Springer Nature remains neutral with regard to jurisdictional claims in published maps and institutional affiliations.